Journal of Nuclear Materials 392 (2009) 341–352

Contents lists available at ScienceDirect

Journal of Nuclear Materials

journal homepage: www.elsevier.com/locate/jnucmat

Perspectives on radiation effects in nickel-base alloys for applications in advanced reactors ☆

A.F. Rowcliffe, L.K. Mansur *, D.T. Hoelzer, R.K. Nanstad

Materials Science and Technology Division, Oak Ridge National Laboratory, Oak Ridge, TN 37831-6138, USA

A B S T R A C T

Because of their superior high temperature strength and corrosion properties, a set of Ni-base alloys has been proposed for various in-core applications in Gen IV reactor systems. However, irradiation-performance data for these alloys is either limited or non-existent. A review is presented of the irradiation-performance of a group of Ni-base alloys based upon data from fast breeder reactor programs conducted in the 1975–1985 timeframe with emphasis on the mechanisms involved in the loss of high temperature ductility and the breakdown in swelling resistance with increasing neutron dose. The implications of these data for the performance of the Gen IV Ni-base alloys are discussed and possible pathways to mitigate the effects of irradiation on alloy performance are outlined. A radical approach to designing radiation damage-resistant Ni alloys based upon recent advances in mechanical alloying is also described.

1. Introduction

Key materials issues for advanced fission reactors, in particular the Gen IV reactors, have been described in a number of recent reports [1–4], and also compared to the corresponding needs for fusion reactors and spallation neutron sources [5]. Structural alloys in these systems are required to maintain structural integrity to doses ranging from tens to hundreds of dpa while operating at high temperatures in order to achieve higher thermal efficiencies [6]. For the core components of the supercritical water reactor (SCWR), and sodium fast reactor (SFR), normal operating temperatures range from 300 to 620 °C, whereas for the gas-cooled fast reactor (GFR) and the lead-cooled fast reactor (LFR), the operating temperature range is approximately 450–850 °C. For the very high temperature reactor (VHTR), normal operating temperatures range from 600 to 900 °C. (The VHTR is also termed the next generation nuclear plant (NGNP) in the US).

Because of their generally higher creep strength compared to austenitic and ferritic–martensitic steels, Ni-base alloys have been proposed for Gen IV in-core components that will experience temperatures higher than about 600 °C. In the present paper, we re-examine some of the past work on radiation effects in Ni-base alloys; because of its importance, we also include a discussion of Alloy 800 which is an Fe-base alloy containing ~33%Ni. Much of the work covered here was carried out in the US National Cladding and Duct program for the liquid metal cooled fast breeder reactor (LMFBR), which was pursued by the US Department of Energy in the approximate timeframe 1974–1982 [7,8]. Extensive research was carried out by programs in the EU during that period and particular aspects of that work are also summarized here.

Compared to austenitic stainless steels and ferritic–martensitic steels, there is much less experience with radiation effects on the Ni-base alloys. However, the available information indicates that essentially all of the commercial Ni-base alloys investigated suffered a significant reduction in tensile ductility during neutron irradiation in the range 400–600 °C for neutron doses approaching 10–15 dpa. A number of these alloys also showed substantial levels of swelling at high doses even though their Ni contents exceeded 40 wt%. Thus, it is clear that radiation effects can impose severe limitations on possible operating parameters in terms of neutron dose and allowable stresses and temperatures. However, based on an analysis of the microstructural evidence related to loss of ductility and swelling resistance, it is possible to suggest two approaches to mitigating the effects of neutron irradiation on the ductility and dimensional stability of Ni-base alloys. A near term evolutionary approach involves modifying the composition and thermo-mechanical processing of existing commercial alloys with the objective of controlling the development of radiation-enhanced and radiation-induced intermetallic and carbide phases and incorporating a high density of trapping sites to disrupt the migration of helium and other undesirable elements to grain boundaries. Such an approach will require the development of new thermodynamic and kinetic models of phase transformations for cascade damage environments. A second, and longer-range revolutionary approach is to design entirely new Ni-base alloys around the concept of

☆ Research sponsored by the US Department of Energy, under contract DE-AC05-00OR22725 with UT-Battelle, LLC.

* Corresponding author. Tel.: +1 865 574 4797.
E-mail address: mansurlk@ornl.gov (L.K. Mansur).

0022-3115/$ - see front matter © 2009 Elsevier B.V. All rights reserved.
doi:10.1016/j.jnucmat.2009.03.023

mechanical alloying. Under certain conditions, it is possible to produce extremely high densities of solute nanoclusters which have been shown to possess extraordinary thermal stability and to convey very high levels of creep resistance. Initial work based on ferritic Fe–Cr alloys indicates that nanoclusters are also remarkably effective traps for both point defects and helium atoms.

2. Background

Several neutron irradiation studies were carried out on commercial Ni-base alloys, including Alloys 600, 625, 702, 718, 800, 706, PE16, Hastelloy X, and Rene 41, in the 1958–1974 timeframe [9–14]. We note that the first six of these alloys are very often designated in both the research literature and by commercial suppliers as Inconel or Incoloy, for example Inconel 718 or Incoloy 800. Severe reductions in tensile ductility were encountered in elevated temperature post-irradiation tests. These unfavorable results were generally ascribed to helium embrittlement with little or no direct microstructural evidence from scanning or transmission electron microscopy. Subsequently, the Ni-base superalloys were selected as the initial focus of an effort to develop cladding and duct alloys for the sodium-cooled fast breeder reactor programs that were vigorously pursued in the US [7,8], and in Europe. These alloys formed one of several approaches to overcoming the void swelling problem discovered in the 300 types of austenitic stainless steels. They were selected on the basis of strength and creep resistance up to 650–700 °C, compatibility with sodium and evidence of swelling resistance derived from charged particle irradiation studies. These advantages were coupled with an extensive experience in processing, fabrication and joining in non-nuclear industries. However, it was found that a wide range of both commercially available and experimental alloys exhibited low ductility failures during tensile tests following neutron irradiation in the range 450–650 °C. This experience led to the abandonment of the Ni-base superalloys in the US program, and efforts to solve the void swelling problem were focused instead on the development of swelling-resistant austenitic stainless steels and on the ferritic–martensitic steels containing 9–12% Cr. More recently, Ni-base alloys have been suggested for potential applications in Gen IV reactors [1,15]. For applications in the VHTR and GFR, their high temperature creep resistance and corrosion resistance at temperatures above 700 °C in non-nuclear environments provide a compelling incentive. Potential in-core applications in high performance light water reactors have also been considered [16]. An in-depth assessment of the potential applications for Ni-base alloys in the Prometheus space reactor system was carried out recently by Angeliu et al. [17]. Swelling resistance and radiation-induced ductility loss were reviewed with a focus on PE16 and Hastelloy X for reactor vessel applications at ~625 °C and neutron doses up to ~8 dpa and specific recommendations were made on mitigating radiation-induced embrittlement based on compositional modifications designed to lower the helium generation rate.

The radiation effects database on commercial alloys is rather limited and information over a significant range of doses and temperatures is restricted to three alloys, namely Alloy 718, Alloy 706 and Alloy PE16. The US Cladding and Duct Program developed a substantial database for these materials based on fast reactor neutron irradiation experiments over the range 450–700 °C and 10–40 dpa. The information developed included (a) tensile behavior, (b) swelling behavior and the evolution of the void and dislocation microstructure, and (c) radiation-enhanced and radiation-induced changes in the precipitate microstructure. The US program also pursued a series of experimental alloys based on compositional and microstructural variants of the commercial alloys, which yielded significant high dose information on embrittlement mechanisms [18]. Swelling behavior was determined for most of these alloys and also for a comprehensive set of pure Fe–Cr–Ni ternary alloys.

During this timeframe, fundamental mechanistic studies on the radiation response of the Fe–Ni–Cr alloy system were pursued in the US basic energy sciences radiation effects program. This work included theoretical modeling and irradiation experiments employing both ion and neutron irradiations focused on swelling behavior, precipitation and microstructural evolution. A more systematic understanding of the relationships between composition, phase stability, microstructural evolution and swelling behavior was developed as a result of this long term basic research [19–22].

In the following we present an evaluation, based mainly on data from the US LMFBR Cladding and Duct Program, of the mechanisms involved in radiation-induced ductility loss and in the loss of swelling resistance in Ni-base alloys. This information is used to assess the potential behavior of the Ni-base alloys currently being considered for the wide range of neutron dose and temperature conditions for the Gen IV reactor systems and to recommend potential avenues for mitigating the effects of neutron irradiation on the performance of these alloys.

3. Radiation-induced ductility loss in Ni-base alloys

During the 1956–1975 timeframe, data on irradiated tensile properties were reported for several Ni-base alloys irradiated in materials test reactors over the range 250–650 °C [1–6]. These early studies included Alloys 600, 625, 706, 718, 800, Hastelloy X, A-286, and Rene 41. Significant radiation-induced reductions in total elongation were observed in elevated temperature testing of all the alloys studied. In general there was little or no microstructural characterization either before or after irradiation; grain boundary helium was invoked as the major factor in ductility loss but without any direct microstructural evidence.

A more intensive investigation of the irradiation performance of the Ni-base alloys was initiated with the advent of the LMFBR materials programs in Europe and in the US [7,8] in the early 1970s. The data generated by the US program were reported in a series of quarterly progress reports issued by the US National Cladding/Duct Materials Development Program. These reports (TC-160 series) are now available for general use. Fast reactor irradiation experiments in both EBR-II and in FFTF were carried out for a wide range of both commercial and experimental Ni-based alloys. Pre- and post-irradiation characterization and analysis yielded a significant level of understanding of the mechanisms involved in the loss of high temperature ductility during post-irradiation tensile testing of these alloys. In addition, a limited amount of information on the behavior of fast reactor mixed-oxide fuel pins with Alloy 706 cladding was obtained, and an extensive database on the performance of mixed-oxide fuel pins with PE16 cladding was developed within the European program. In the following, some of the fast reactor irradiation data for alloys Alloy 718, Alloy 706 and Alloy PE16 are used to illustrate the principal features of radiation-induced ductility loss in nickel-based alloys.

Neutron doses are expressed throughout in terms of displacements per atom (dpa). Most of the data referred to here were derived from experiments in the EBR-II and FFTF reactors and the neutron exposure data has been converted using the approximate relationship of 1.0×10^{26} n/m^2 ($E > 0.1$ MeV) = 5 dpa. All compositions are given in units of wt%.

4. Alloy 718

The primary strengthening phases in Alloy 718 (19Fe–18Cr–53Ni–2.5Mo–5.0Nb–0.9Ti–0.6Al–0.04C) are the metastable gamma

double prime {bct, Ni_3Nb} and gamma prime {$L1_2$, $Ni_3(TiAl)$}. During thermal aging at $\geqslant$650 °C these phases coarsen and eventually transform to the more stable forms of delta {orthorhombic, Ni_3Nb} and eta phase {hcp, Ni_3Ti}. Other phases which often develop and play significant roles in determining mechanical behavior include the α-Cr and σ-phase and the carbides, MC, $M_{23}C_6$, and M_6C. Several heat treatments involving double aging are utilized to adjust the strength level and rupture life depending upon the application. Precipitation behavior and phase stability in Alloy 718 and the influence of small variations in the concentrations of elements such as Ti, Al, and Nb have been the subject of several recent investigations [23–26].

Within the US National Cladding/Duct Materials Development Program, an initial survey of the irradiation behavior of a wide range of both commercial and experimental Ni-base alloys was carried out to neutron doses of 9, 20, and 34 dpa over the temperature range 450–735 °C; post-irradiation tensile testing was carried out over a range of temperatures at a strain rate of $\sim 4 \times 10^{-4}\ s^{-1}$ [27,28].

Fig. 1 illustrates the temperature dependence of hardening for Alloy 718 in a solution treated (ST) condition. For a dose of 20 dpa, hardening persisted up to ~600 °C and then decreased with increasing irradiation temperature, becoming negligible at 735 °C. Ductility values were strongly reduced by irradiation with a ductility trough at 550–625 °C in tests carried out at the irradiation temperature. In this range, failures occurred at maximum load with total and uniform strains of 1–2%. An even more severe level of embrittlement was encountered when testing was carried out at temperatures above the irradiation temperature (T_i), in order to simulate possible off-normal temperature excursions in a fuel pin. Under these conditions, failure occurred soon after yielding with uniform and total strains in the range 0.1–0.2%. Fig. 2 illustrates the dependence of total elongation on test temperatures both above and below T_i.

Following irradiation to 34 dpa, ductility decreased further with failures occurring in the elastic range during tensile tests at T_i + 110 °C. Good ductility was retained in all tests for solution annealed specimens irradiated to 34 dpa at 735 °C, which is above the hardening range. In the temperature range where severe loss of ductility occurred, a dense dispersion of gamma prime developed during irradiation together with an array of large (0.1–0.3 μm) platelets of eta phase. Very little grain boundary precipitation occurred and helium bubble formation was limited to a few isolated bubbles 4–6 nm in diameter. Deformation was highly planar and

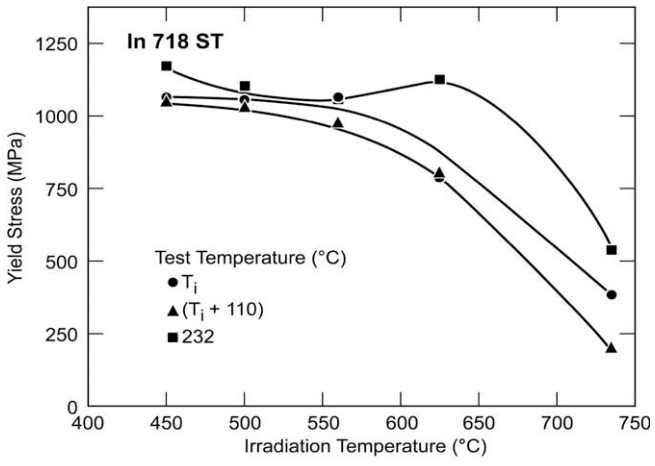

Fig. 1. Yield stress versus irradiation temperature, T_i, for Alloy 718 in the solution treated condition, irradiated to ~20 dpa and tested at three different temperatures. Data from Horak et al. [27].

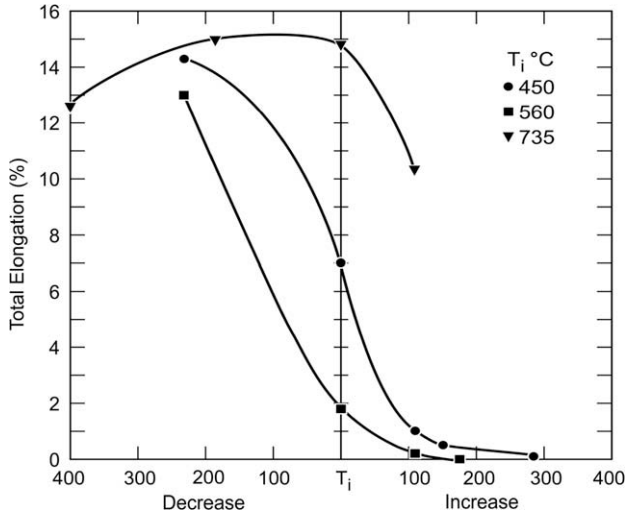

Fig. 2. Variation of ductility with tensile test temperature for Alloy 718 (ST) irradiated at three different temperatures, T_i, to a dose of ~20 dpa. Data from Horak et al. [27].

confined to a limited number of slip bands. Examination of fracture surfaces established that all of the low ductility failures were associated with a predominantly trans-granular fracture mode, probably associated with the decohesion of the eta phase platelets. Auger analysis of in situ fracture specimens indicated the presence of high concentrations of sulfur and phosphorus on the fracture surfaces [29].

In summary, for the solution annealed Alloy 718, there was no evidence linking ductility loss to grain boundary phenomena such as radiation-induced precipitation or helium bubble growth. Instead, the evidence suggested that the interface between the matrix and the eta phase was weakened by radiation-induced segregation of sulfur and phosphorus and possibly by helium bubble formation. During tensile testing decohesion of the interface occurred as a result of the high stress concentrations developed at the intersection of localized slip bands with the eta phase platelets.

5. Alloy 706

Alloy 706 (37Fe–16Cr–42Ni–0.1Mo–2.9Nb–1.7Ti–0.3Al–0.03C) is less highly alloyed than Alloy 718 although the precipitation and strengthening behavior are dominated by the same phases in both alloys. Specimens heat treated for optimum stress rupture properties were irradiated using the same conditions noted above for Alloy 718 [27,28]. The double aging treatment resulted in the development of a nearly continuous eta phase and globular delta phase at the grain boundaries. Within the grains, a dispersion of cuboidal gamma prime particles enclosed by discs of gamma double prime developed during the heat treatment. The unirradiated yield stress was fairly constant at ~920 MPa up to ~650 °C and then decreased rapidly at higher temperatures. The dose dependence of yield stress at five irradiation temperatures is shown in Fig. 3. Radiation hardening further increased yield stresses to >1000 MPa at 450 and 500 °C. At 560 °C, very little change occurred up to 34 dpa and at 625 °C radiation softening occurred related to radiation-enhanced coarsening of the gamma prime/double prime dispersion. Radiation-induced ductility loss was initially not as severe as in Alloy 718 and after irradiation to 20 dpa, total elongations ranged from 1.5% to 3.0% at 450–625 °C in tests conducted at the irradiation temperature. Uniform and total strains were approximately equal with failures occurring at maximum load. However, irradiation to 34 dpa resulted in further reductions in

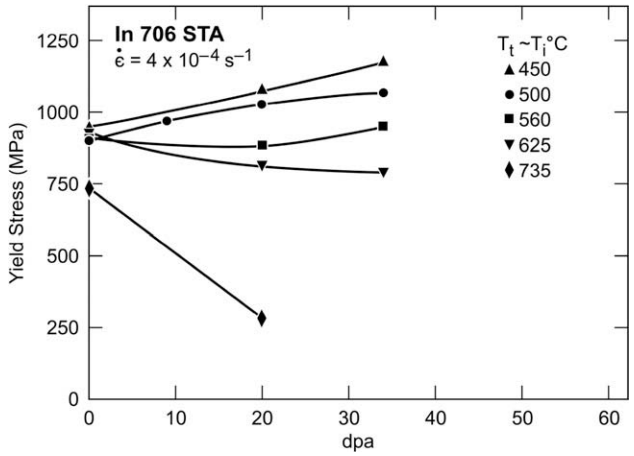

Fig. 3. Neutron dose dependence of yield stress for Alloy 706 irradiated at various temperatures and tested at T_i. Data from Horak et al. [27].

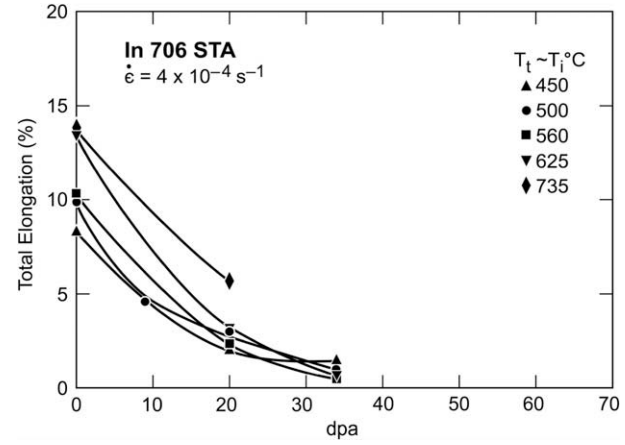

Fig. 4. Neutron dose dependence of total elongation for Alloy 706 irradiated at various temperatures and tested at T_i . Data from Horak et al. [27].

ductility and uniform and total elongation decreased to below ~1% for tests at the irradiation temperature (Fig. 4).

Following irradiation to 20 dpa in the range 500–625 °C, tensile testing at T_i + 110 °C resulted in severe embrittlement with uniform strains reduced to <0.5%. Further irradiation to 34 dpa resulted in fracture occurring before yielding in post-irradiation tensile tests at T_i + 110 °C. In contrast to Alloy 718, the brittle failures were entirely inter-granular for irradiation temperatures at 500 °C and above, in tests at T_i and T_i + 110 °C. SEM examination of the fracture surfaces indicated that separation of the grain boundary eta phase interface with the matrix had occurred. TEM examination revealed the presence of radiation-induced voids associated with the grain boundary eta phase [28]. As with the Alloy 718, deformation was highly localized in the low ductility regime. The release of helium was detected during in situ fracture in an Auger facility and the presence of high concentrations of sulfur and phosphorus were detected on fracture surfaces [29].

In related work, a regime of low ductility inter-granular failure in Alloy 706 was demonstrated in post-irradiation ring crush tests in which irradiated sections of tubing were subjected to intense local bending [30,31]. In this instance, cladding specimens were irradiated to ~25 dpa in a solution treated condition and therefore the grain boundary eta phase and intra-granular gamma prime and double prime phases were not initially present. Brittle failures occurred following irradiation at 560, 610, and 660 °C in tests conducted above 550 °C. Brittle failure was attributed in this instance to the radiation-enhanced formation of a continuous grain boundary film of gamma prime precipitation containing Al, Ti, and Si [31].

Brittle failures occurred in a set of mixed-oxide fuel pins clad with Alloy 706 (in a solution treated condition), during irradiation to ~5 at.% burn-up, equivalent to ~25 dpa [32,33]. Inter-granular brittle failure was related to the radiation-enhanced development of continuous grain boundary eta phase at temperatures ranging from 450 to 650 °C [33]. TEM examination failed to detect either the presence of grain boundary gamma prime or the existence of grain boundary helium bubbles.

6. Alloy PE16

Alloy PE16, (33Fe–17Cr–44Ni–3.7Mo–1.2Ti–1.3Al–0.05C), is less highly alloyed than either Alloy 718 or Alloy 706 and the standard aging treatment produces a dispersion of gamma prime only, with grain boundary particles of $M_{23}C_6$. Radiation-induced loss of ductility was initially detected in PE16 following irradiation to low (<2 dpa) displacement doses in mixed spectrum test reactors [34]. In this environment, the high thermal neutron flux ensures the complete burn-up of the ^{10}B isotope initially present in the alloy and the generation of significant concentrations of helium. Overlapping of the alpha particle recoil spheres which surround boron-rich grain boundary particles can lead to local grain boundary clustering and coarsening of helium bubbles [35]. Loss of tensile ductility for test temperatures >650 °C was shown by Broomfield [34] to correlate directly with increasing thermal fluence and boron burn-up. Fracture toughness measurements, reported by Nicholson and Jones [36] on highly constrained compact tension specimens, demonstrated severe reductions in K_{1c} following irradiation to <1 dpa in a mixed spectrum reactor at temperatures of 500 and 700 °C. Transmutation of the ^{10}B isotope resulted in helium concentrations in the range 17–24 appm and the deterioration in fracture toughness was attributed to helium bubble growth and coalescence on grain boundaries subjected to a critical level of stress.

Subsequent investigations under the US and European LMFBR materials development programs focused on the effects of irradiation in fast reactor environments in which high levels of radiation hardening occurred over the range 400–600 °C. The major sources of helium in this environment are the threshold (n,α) reactions with the major alloying elements. Ni has the largest cross-section and thus the helium generation rate scales with Ni content; for PE16 the helium generation rate from this source is ~1.2 appm/dpa. Depending on core position, additional helium may be generated from low energy (n,α) reactions with ^{10}B and $^{58}Ni/^{59}Ni$.

The irradiation behavior of PE16 has been widely reported in the literature. The investigation reported by Bajaj et al. [37] provides a fairly comprehensive illustration of the principal effects of neutron dose and irradiation temperature on the tensile behavior. Flat sheet tensile specimens in a fully aged condition were irradiated in EBR-II to doses of 8, 19, 34, and 45 dpa at temperatures ranging from 450 to 735 °C. For tests carried out at the irradiation temperature, the magnitude of the radiation hardening was fairly constant from 450 to ~625 °C and then decreased rapidly with increasing irradiation temperature. Radiation hardening apparently saturated below 9 dpa (Fig. 5). Total elongation was lowered by irradiation at all temperatures. The magnitude of the reduction increased strongly with temperature up to ~550 °C and then remained fairly constant with further increases in irradiation temperature (Fig. 6).

Tensile testing at T_i + 110 °C resulted in a more drastic loss in ductility. After irradiation to 19 dpa in the range 500–625 °C, grain

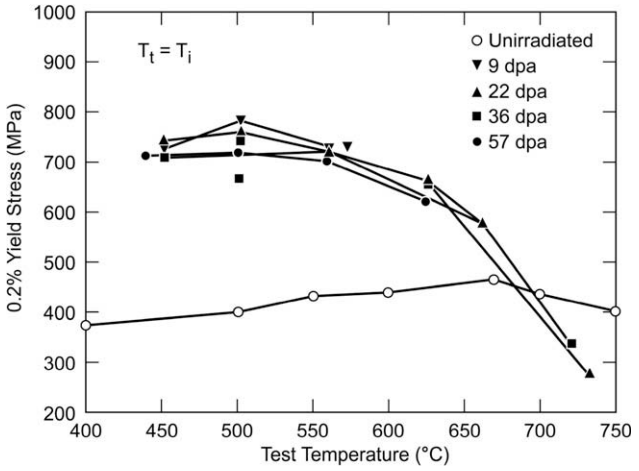

Fig. 5. Neutron dose and temperature dependence of yield stress for Alloy PE16 in a solution treated and aged condition; tensile tested at T_i. From Bajaj et al. [37].

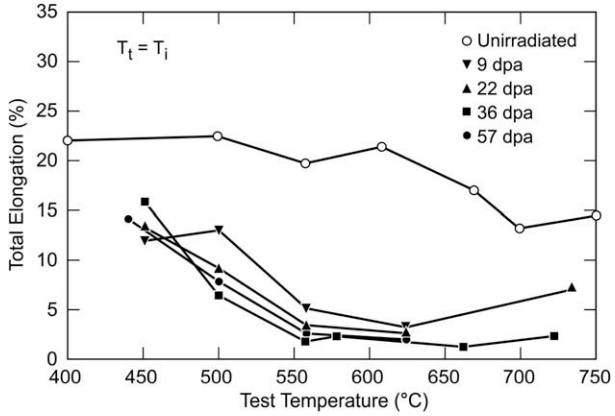

Fig. 6. Neutron dose and temperature dependence of ductility for Alloy PE16 (STA); tensile tested at T_i. From Bajaj et al. [37].

boundary failure occurred after a limited amount of strain hardening with uniform and total elongations in the range 0.3–0.7%. Further irradiation to 32 dpa in this temperature range resulted in brittle failure in the elastic range during tensile tests carried out at $T_i + 110$ °C. Brittle grain boundary failures were also reported by Vaidyanathan et al. [30] in ring compression testing of solution treated PE16 when tests were carried out above the irradiation temperature following irradiation to ~35 dpa at 554 °C.

In summary, brittle grain boundary failures in PE16 have been variously ascribed to (a) radiation-induced hardening and the difficulty of relieving triple point stresses due to grain boundary sliding [37], (b) brittle failure of radiation-induced continuous grain boundary films of a gamma prime phase [38], and (c) mechanisms related to the behavior of grain boundary helium bubbles [39,40]. It was pointed out by Boothby [41], that the re-distribution of gamma prime and the formation of a continuous film at grain boundaries are strongly dependent on the initial heat treatment; continuous grain boundary gamma prime is only observed in solution treated materials and does not occur in fully aged material. Grain boundary embrittlement in PE16 has been observed both with and without the formation of grain boundary gamma prime, and the dominant embrittlement mechanism is probably related to helium bubble growth [41] based upon the stress-induced instability criteria originally proposed by Hyam and Sumner [42].

In spite of the evidence cited above for the potential for catastrophic ductility loss, the performance of mixed-oxide fuel pins utilizing PE16 cladding has been surprisingly good [43–46]. Approximately 75% of the core of the PFR at Dounreay was loaded with PE16 clad fuel pins operating in the range 400–650 °C and achieved burn-up levels of ~20 at.% (~80 dpa) without a single failure. This experience suggests that with the correct fuel pin design, it is possible to avoid subjecting the cladding to the high stress-temperature regime in which grain boundary failures occur. For the PFR fuel pins, the maximum hoop stress due to fission gas pressure was estimated to be < 70 MPa, which is a factor of 2–3 less than the stress required to induce unstable growth of the observed grain boundary helium bubbles [41].

7. Void swelling in Ni-base alloys

The early work of Johnston et al. [47] utilizing 4 MeV Ni ion irradiation, demonstrated a strong compositional dependence of swelling in the Fe–Cr–Ni ternary system. Even after irradiation to 140 dpa at 675 °C, a regime of zero swelling was observed over a region of compositional space embracing 7–20 wt% Cr and 45–75 wt% Ni. Subsequent neutron irradiation experiments by Bates and Johnston [48] to doses up to 15 dpa confirmed the general trends of this work. However, as higher neutron doses were achieved in subsequent reactor experiments, it became apparent that the heavy ion data were misleading, particularly at lower temperatures, and it was shown that a number of physical factors unique to the heavy ion irradiation environment combine to distort the temperature dependence of swelling and to depress the steady state swelling rate [49,50]. High dose neutron irradiation experiments, summarized by Garner and Brager [51], demonstrated that the region of composition space in which the incubation dose for swelling extended to ~100 dpa was not as extensive as indicated by the ion irradiation data. In ternary alloys containing 15 wt% Cr irradiated in a fast reactor to ~100 dpa at temperatures in the range 538–650 °C, swelling was limited to <5% for alloys containing 40–50 wt% Ni. Outside of this composition range, steady state swelling rates reached ~1%/dpa once the incubation dose was exceeded (Fig. 7).

Although adjustment of the Ni content remains an important tool in the design of low-swelling alloys, other compositional and microstructural factors can exert an equally important and sometimes

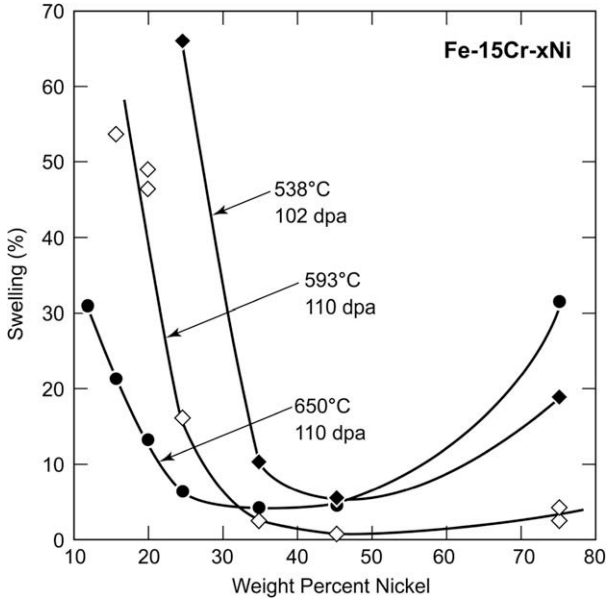

Fig. 7. Swelling behavior of Fe–Cr–Ni ternary alloys, neutron irradiated to ~100 dpa. From Garner and Brager [51].

over-riding influence on swelling behavior. In particular the distribution of second phase particles and their stability in the radiation environment is a dominant factor in determining the extent of the low-swelling incubation regime. Second phase particles can influence the nucleation and growth of cavities in several ways depending on their size, number density, and the nature of the particle-matrix interface. For example, a high number density of particles can be effective in extending the incubation swelling regime by, (a) pinning and maintaining a steady state dislocation network, (b) acting as efficient sinks for point defects, or (c) trapping helium at the particle/matrix interface. On the other hand, the development of large inter-metallic or carbide phases can terminate the incubation regime via the precipitate-point defect collector effect [52], in which the interface serves as an efficient sink for helium and vacancies to achieve concentrations sufficient to nucleate critical-size, gas-stabilized cavities. The precipitate-cavity pair is a stronger sink for point defects than an isolated cavity and the precipitate and associated cavity undergo synchronized growth. The precipitation of a large volume fraction of intermetallic or carbide phases can also significantly deplete the matrix of solutes such as C and Si which tend to inhibit swelling while they are in solution [50].

The US National Cladding/Duct Program investigated the swelling behavior of a very wide range of commercial alloys as part of a screening program carried out in parallel with the investigation of the pure ternary alloys. For illustrative purposes a sub-set of the swelling data presented by Garner and Gelles [53] is shown in Table 1 for fast reactor irradiation at temperatures ranging from 400 to 650 °C and for neutron doses in the range 70–114 dpa. These data provide a good illustration of the diversity of the swelling response of the Ni-base alloys. The gamma prime/gamma double prime Alloys 718 and 706 may be classified as low-swelling alloys since swelling is clearly in the incubation regime for all temperatures and doses. However Alloy PE16, with essentially the same Ni content as Alloy 706 is clearly moving out of the incubation regime at 510–558 °C with swelling approaching 5% at ~100 dpa. Both Hastelloy X and Alloy 800 are a completely different story however, and provide an important example of how microstructural factors can dominate the swelling-inhibiting effects of a high Ni content, particularly in the case of Hastelloy X which contains ~50 wt% Ni. The latter alloy exhibits a strong high temperature swelling peak with swelling approaching 80% at 593 °C. Alloy 800 exhibits double-peak swelling behavior with maxima at 427 and 510 °C. Although there is no direct microstructural evidence at these high doses, the available information from thermal aging and from low dose neutron irradiation [54] indicates that the loss of swelling resistance in these two alloys is probably related to phase instabilities involving the precipitation of carbon. Both of these alloys develop extensive inter-granular and intra-granular precipitation of the carbide phases M_6C and $M_{23}C_6$ during thermal aging in the 600–900 °C range [55,56].

The probable role of the M_6C and $M_{23}C_6$ phases may be inferred from the extensive work carried out on the irradiation-induced microstructural changes in the 300-series stainless steels. In 316 stainless steel, these phases have complex compositions containing Cr, Ni, Fe, Mo, and Si with minor quantities of Ti, Mn and V. While the compositions that develop during either thermal aging or during irradiation are very similar [57], the kinetics of precipitation are enhanced during irradiation by the point defect-enhanced diffusivities to the extent that precipitation of M_6C during neutron irradiation has been observed at temperatures as low as ~380 °C [57]. The large rhombohedral morphology that develops above ~500 °C in stainless steels provides an ideal site for the rapid development of critical-sized cavities via the collector effect mechanism [52]. In the absence of any detailed microstructural information it is difficult to interpret the appearance of the low temperature swelling peak in Alloy 800 and the low temperature densification observed in Hastelloy X. However, based on the experience with stainless steels, it seems likely that the differences in the swelling behavior between these alloys are related to differences in the nature and morphology of the various phases resulting from the radiation-enhanced precipitation of carbon.

8. Discussion

8.1. Implications for the performance of Ni-base alloys in Gen IV systems

In the foregoing, data from the earlier LMFBR cladding and duct materials programs was used to highlight some of the mechanisms involved in both the loss of high temperature ductility and the loss of swelling resistance under fast reactor irradiation conditions. For wrought commercial alloys with Ni contents in the 35–55% range, phase instabilities frequently play a dominant role in both radiation-induced ductility loss and in the termination of the swelling incubation regime. Precipitation of micrometer-scale plate and block morphologies, both inter-granular and trans-granular, are potential sites for crack initiation particularly in the radiation-hardening regime. The breakdown of swelling resistance appears to be related to the radiation-enhanced formation of large carbide particles of various types which form effective sites for helium and point defect trapping leading to the co-operative growth of particle-cavity entities [52]. Under certain conditions, the radiation-induced segregation to grain boundaries of solute species such as Ni, Si, Ti and Al, leads to the formation of continuous films of gamma prime. Radiation-induced segregation of P and S may also play a role in reducing the strength of particle-matrix interfaces and grain boundaries. Helium is frequently implicated in low ductility failures related to the stress-induced growth of grain boundary helium bubbles, a phenomenon which is manifested primarily at temperatures well above the hardening regime. More than one of these mechanisms may be operative, particularly when testing is carried out at temperatures above or below the irradiation temperature.

Of the commercial Ni-base alloys for which there is a significant radiation effects data base, Alloy PE16 clearly possesses the best combination of swelling resistance, phase stability, high temperature strength and creep rupture life. There is also an extensive database on processing, heat-to heat variability and fuel pin fabrication

Table 1
Swelling (%) in commercial Ni-base alloys; neutron irradiation data from Garner and Gelles [53].

Irr. temp. (°C)		399	427	454	483	510	538	593	650
Neutron dose (dpa)		72	93	70	89	108	104	114	113
Alloy	Ni (wt%)								
800	34	10.8	41.1	1.9	5.5	47.2	11.9	–	14.6
706	42	0.2	0.2	0.1	−0.1	0.0	0.0	0.1	–
PE16	43	0.1	0.4	1.1	2.5	4.7	4.5	1.3	0.1
HAST X	50	−3.1	−2.3	−3.0	0.9	15.9	38.0	79.9	–
718	53	0.4	0.1	0.2	0.2	0.1	0.3	0.0	−0.1

Table 2
Nominal compositions (wt%) of commercial Ni-base alloys.

Alloy	Ni	Fe	Cr	Mo	Nb	Co	W	Ti	Al	C
800H	33	45	21	–	–	–	–	0.4	0.4	0.08
120	37	33	25	–	0.7	3.0	–	–	0.1	0.05
706	42	37	16	0.1	2.9	–	–	1.7	0.3	0.03
PE-16	43	33	17	3.7	–	–	–	1.2	1.3	0.05
617	45	23	20	–	–	10.0	–	0.6	0.8	0.05
Hastelloy X	50	17	22	9.0	–	1.0	0.6	–	–	0.15
718	53	19	18	2.5	5.0	–	–	0.9	0.6	0.04
230	55	3	22	2	–	4	14	–	0.3	0.10

coupled with a record of successful fuel pin performance. This comprehensive experience provides a sound basis for the evaluation of the performance of conceptual designs for in-core components in Gen IV systems utilizing a Ni-base alloy. However, the upper operating temperature limit for PE16 is probably in the range 650–700 °C, and for many situations higher strength at higher temperatures will be required.

A variety of high strength Ni-base alloys are currently being evaluated for in-core and core support applications in potential Gen IV reactor systems [58]. These include Alloy 617, Hastelloy X, Hastelloy XR, and Alloy 230 for applications above ~760 °C, and Alloys 120 and 800H for applications in the 650–760 °C range, (Table 2). Of these alloys only Alloy 800H is qualified for nuclear service under the ASME B&PV Code Subsection NH. It is important to note that there are no neutron irradiation performance data for Alloy 230 and Alloy 120, and irradiation data for Alloy 617 are limited to ~1.5 dpa. For Alloy 800 and Hastelloy X, there are sufficient data to indicate that both alloys are susceptible to radiation-induced loss of ductility in certain regimes of dose and temperature. However post-irradiation microstructural characterization has not been sufficiently rigorous to define the relative significance of phase instabilities, solute segregation, radiation hardening and helium generation. Consequently the mechanisms of ductility loss have not been convincingly identified. Regarding swelling behavior however, there are sufficient high fluence reactor data to make a reasonable assessment of the potential swelling behavior in the in-core environment of the fast and mixed spectrum Gen IV reactor concepts under consideration. As discussed above, the swelling resistance of both Alloy 800 and Hastelloy X is poor and it is reasonable to conclude that the application of these alloys for temperatures in the range 400–650 °C will be severely limited by the rapid breakdown in swelling resistance triggered by the radiation-enhanced precipitation of several carbide phases and the co-operative growth of attached cavities [52]. Alloy 617 is very similar to Hastelloy X in terms of general phase transformation behavior and precipitation kinetics. Time–temperature-precipitation diagrams for both alloys have been determined by Kirchover, et al [59] and subsequently the diagram for Hastelloy X was extended by Zhao et al. to include the precipitation of the sigma and mu phases [60]. For both alloys, fine dispersions of coherent and semi-coherent phases do not develop on a scale sufficient to affect the overall point defect sink strength and contribute to swelling resistance. Instead, precipitation over a wide temperature range is dominated by the formation of M_6C and $M_{23}C_6$ distributed on a fairly coarse scale. This strongly suggests that during fast neutron irradiation, Alloy 617 will also undergo a transition into a steady state swelling regime at a relatively modest neutron dose level and at temperatures determined by the radiation-enhanced precipitation kinetics of complex carbide phases. Thermal aging studies of Alloy 230 indicate that precipitation behavior is similarly dominated by the formation of $M_{23}C_6$ and M_6C on a fairly coarse scale. There is therefore a distinct possibility that this alloy may also be susceptible to a loss of swelling resistance in the 400–650 °C range related to the radiation-enhanced precipitation and the co-operative growth of voids attached to the precipitate surfaces. Further consideration of these alloys for Gen IV applications involving significant levels of displacement dose should therefore include an early exploration of their swelling resistance.

The available evidence suggests that the group of Ni-base alloys currently being considered for Gen IV applications will require a significant degree of compositional re-structuring and microstructural design to minimize the radiation -enhanced and radiation-induced formation of micrometer-scale carbide and intermetallic phases and to promote the formation of finely-dispersed phases such as MC, gamma prime, M_3P etc., to enhance the trapping of both point defects and helium atoms and to inhibit recovery of the dislocation structure. Stabilization of carbon utilizing the Group IV and V reactive elements would appear to be an important avenue of exploration in seeking to improve the irradiation performance of these alloys.

In recent years, computational thermodynamics has evolved as a powerful means of describing phase equilibria in multi-component systems as a function of alloy composition and temperature [61]. Basic thermodynamic calculations may be combined with kinetic analyses to describe the approach to equilibrium when behavior is diffusion-controlled and such calculations have been extensively applied to the Ni-base superalloys [62]. However, in order to successfully model phase stability during long term exposure in a radiation environment, it will be necessary to develop methodologies to incorporate not only the enhanced diffusion rates related to the concentrations of mobile point defects, but also the development of persistent solute-concentration gradients (i.e. radiation-induced segregation) which frequently leads to the formation of non-equilibrium, radiation-induced phases at point defect sinks [57].

Ni-base alloys are also being considered for the structural components of thermal spectrum reactors epitomized by the VHTR; these include the core barrel, core support, inside shroud, and upper core restraint. For these components the maximum doses accumulated over a 50–60 year lifetime are not expected to exceed a few dpa. Consequently, many of the radiation effects discussed in the foregoing (radiation hardening, flow localization, void swelling and irradiation creep), are unlikely to have any significant impact on alloy performance. There are however several issues related to the irradiation environment that will need to be evaluated such as helium generation, radiation-induced solute segregation and radiation-induced changes in long-term phase stability. Because of the high operating temperatures and the potential for very high off-normal temperatures, the generation of helium and the subsequent migration and clustering to form gas bubbles needs to be carefully assessed. The primary sources of helium for VHTR components stem from the high thermal neutron cross sections for the (n,α) reactions with the ^{58}Ni, ^{59}Ni and ^{10}B isotopes. Although detailed calculations of helium production from these sources have not been carried out for the VHTR, thermal fluxes in the 10^{18} n/m^2/s regime could lead to helium generation of the order of 10–50 appm over component lifetimes, which is sufficient to affect grain boundary integrity at certain combinations of temperature and stress. At the very high temperatures and extremely long lifetimes envisioned for some VHTR components, it is conceivable that helium concentrations as low as ~5–10 appm could induce grain boundary embrittlement for structures operating under sufficiently high stresses. Additional work is required to investigate the helium embrittlement process at high temperatures and low helium levels in candidate structural alloys. An important first step therefore is to carry out detailed calculations of helium generation from all sources as a function of time and core position for the prime candidate alloys Alloy 617, Alloy 230, Hastelloy X and Alloy 800. Information on the initial concentration and microstructural distribution of boron for each alloy will also be required. High

temperature reactor irradiation experiments designed to produce relevant helium concentrations will be needed to develop information on the mobility of helium atoms and the nucleation and growth of helium bubbles. Experimental data on candidate alloys and on simple model alloys will be required to support the development of reliable models of helium behavior in microstructures containing various types of sinks.

At this juncture, there is little information on the possible range of stresses which could be imposed on the various metallic core components. Both primary static loads and secondary loading from thermal stresses need to be evaluated to provide a basis for modeling the possible growth kinetics of grain boundary helium bubbles and to ensure that post-irradiation mechanical testing is carried out in appropriate loading regimes. If it is established that helium generation poses a potential threat to the load-bearing capacity of the candidate alloys in their present form, then there are several strategies, based on the earlier work on grain boundary helium embrittlement, that could be pursued to either modify the composition (e.g. restriction of boron levels), or to select a composition and microstructure designed specifically to delay or to prevent the development of an array of critical-sized grain boundary helium bubbles. Possible approaches would include, (a) the development of radiation-stable finely dispersed phases with particle/matrix interfaces optimized to trap helium, (b) the introduction of a dislocation network via cold work, (c) the development of grain boundary microstructures designed to trap helium on a fine scale at particle/matrix interfaces and (d) heat treatments designed to provide suitable second phase grain boundary particles, or isolated regions of recrystallized matrix (necklace structure), to impede the propagation of helium-driven cracks.

Another potential avenue which could be explored, initially through modeling, is grain boundary engineering. For example, it has been shown that special grain boundaries with low coincidence site lattice relationships sometimes display a high resistance to inter-granular sliding and cavitation [63]. The beneficial effects of grain boundary engineering on the corrosion resistance and strength of Alloy 800H and Alloy 617 have been reported recently [64,65].

It is also possible that the radiation environment of the VHTR could influence long term phase stability in Ni-base alloys. Although the displacement rate is very low, the exposure time is very long and it is possible that the kinetics of particle coarsening and phase compositions could be affected by the relatively low rate of cascade events. These possibilities need to be addressed by advanced modeling techniques coupled with well designed low flux neutron irradiation experiments.

For components operating at sufficiently low temperatures, it is possible that radiation-induced solute segregation could significantly influence microstructural development even at low neutron doses, depending upon alloy composition. A case in point is the application of Alloy 800H for control rod cladding operating in the 500–630 °C range. Low dose neutron irradiation of Alloy 800 in the 400–600 °C temperature range often induces a significant reduction in uniform and total elongation in post-irradiation tensile tests, with ductility decreasing strongly with increasing test temperature [66,67]. In these situations, helium could be playing a role in reducing grain boundary strength with ductility loss occurring at He levels of only 1–2 appm. The Alloy 800 specification allows up to 1.2 wt% (Ti + Al) and the precipitation of gamma prime during thermal aging of some heats at 525–560 °C is well-documented [68]. It is likely therefore that for some heats, radiation-enhanced precipitation of gamma prime, $Ni_3(Ti,Al)$, will occur at even lower temperatures during neutron irradiation; the formation of a radiation-induced Ni_3Si is also a strong possibility. Segregation of the gamma prime-forming elements and impurity elements such as P and S to grain boundaries is highly probable, particularly since the alloy is put into service in a solution treated condition with a very low initial sink density. In some instances the concentrations of segregating species could be sufficient to compromise grain boundary strength even at low neutron doses.

Although not directly related to radiation effects, the issue of radio-activation and the relationship between alloy composition and the generation of highly activated species needs to be considered as part of the overall alloy development program for Gen IV. From a reactor maintenance and safety point of view, the presence of significant concentrations of Co in several of the candidate Ni alloys such as Alloy 617, (~12 wt%), Alloy 230 (~5 wt%), and Hastelloy X (~1.5 wt%) is a source of highly radioactive contamination of the primary coolant system via the erosion of oxide particles from the surface of the major metallic structural components. An additional concern is that extremely high levels of radioactivity will necessitate greatly increased safety requirements and amplify the costs of carrying out mechanical property, dimensional and microstructural measurements during alloy qualification irradiation programs.

8.2. Design of radiation damage-resistant alloys via mechanical alloying

A more radical approach to developing Ni-base alloys with improved tolerance to radiation damage and extended high temperature performance is to utilize mechanical alloying to produce completely new alloys specifically designed for optimal performance in the various types of Gen IV radiation and chemical environments. During the past 20 years, oxide-dispersion-strengthened alloys based upon ferritic–martensitic and ferritic steels containing dispersions of yttrium oxides (Y_2O_3) have been developed for fast breeder reactor applications and for non-nuclear applications, (e.g., the metal heat-treating industry). These materials were developed via comprehensive and systematic efforts to optimize the composition, the number density and size of oxide particles and by varying the processing parameters involved in the mechanical alloying and powder consolidation stages. In addition, processing parameters were established for the production of high quality thin-wall tubing with isotropic mechanical properties. The development of these technologies for fast reactor applications has been summarized by Ukai et al. [69] and it has been demonstrated that ODS ferritic alloys maintain their outstanding swelling resistance to neutron doses as high as 200 dpa [70]. There is evidence for partial recoil dissolution of the oxide particles after 100 dpa at ~700C [71].

In recent years, mechanical alloying (MA) approaches have been pursued with considerable success in the US, Japan and the EU in an effort to improve the high temperature creep properties of the reduced activation class of ferritic–martensitic steels for structural applications in fusion energy systems. It has been shown recently that it is possible to induce dissolution of the stable oxide particles characteristic of the current ODS alloys and to redistribute the chemical constituents as nano-scale oxygen-rich clusters which dramatically improve high temperature creep resistance. In principle at least, it is possible that the mechanical alloying methodologies being developed within the ferritic–martensitic class of steels could be applied to the Ni-base alloys. If successful, this approach could provide a means of overcoming the deficiencies related to the radiation-induced loss of ductility and swelling resistance observed in many of the Ni-base alloys while retaining or enhancing their excellent corrosion resistance in various media.

The microstructural design for achieving high tolerance to neutron irradiation damage in bcc systems is exemplified by the recently developed advanced dispersion-strengthened nano-structured 14YWT ferritic alloy, which contains a high number density of oxygen-rich nano-size solute clusters (nanoclusters) and

nano-size grains [72–74]. This alloy was produced by the MA method of ball milling a small quantity (0.30 wt%) of Y_2O_3 powder with Ar gas atomized pre-alloyed powder of Fe–14Cr–3 W–0.4Ti (nominal composition in wt%) followed by consolidation of the milled powder by hot extrusion. In this process, the initial Y_2O_3 powder is reduced in size and may ultimately be forced into solution in the bcc α-Fe lattice with high energy ball milling [75,76]. If this occurs, then a high number density of nanoclusters form during consolidation of the milled powder at elevated temperatures. Fig. 8 shows the nanoclusters that form in 14YWT during the MA process. In Fig. 8, the nanoclusters are observed as small dark regions in the Energy-Filtered TEM (EFTEM) Fe–M jump ratio image (Fig. 8(a)) and in separate element maps of Cr, Ti, Y, and O (Fig. 8(b)) acquired by the local electrode atom probe (LEAP). The Fe–M jump ratio image is very sensitive to local differences in the Fe composition; the dark contrast indicates that the nanoclusters are depleted in Fe [77]. Information about the composition and size of the nanoclusters are determined by LEAP using the maximum separation envelope and radius of gyration methods, respectively [78]. Fig. 8(b) shows that the nanoclusters are enriched in Ti, Y, and O, with the Ti and O contents significantly higher than the Y content. The typical analysis of nanoclusters, for example those present in the SM4 heat of 14YWT, shows that the composition is 42.2 ± 5.6% Ti, 7.5 ± 4.3% Y, 43.5 ± 5.3% O, with only 5.5 ± 4.6% Fe and 1.2 ± 1.1% Cr. The size is 2.0 ± 0.4 nm diameter and the number density is $\sim 4 \times 10^{23}$ m^{-3} [72].

Fig. 9 shows that the 14YWT alloy also contains a nano-size grain structure. The grain size observed in the TEM micrograph (Fig. 9(a)) was determined to be 136(±14) nm. The EFTEM Fe–M jump ratio image (Fig. 9(b)) shows that a high number density of nanoclusters preferentially nucleated on grain boundaries, which hindered grain growth at the consolidation temperature. Tensile and fracture toughness testing have shown that the 14YWT alloy possesses excellent high-temperature strength and low-temperature fracture toughness properties, which are attributed to the combination of nanocluster dispersion and nano-size grain structure [72,79].

Similar nanocluster dispersions were discovered in the oxide dispersion strengthened (ODS) 12YWT ferritic alloy that was developed in Japan [80] and the MA957 ferritic alloy that was developed and patented by the International Nickel Company [81] prior to the development of the 14YWT alloy. These two advanced ODS ferritic alloys possess very good high-temperature strength and thermal creep properties [82]. Fig. 10 compares the Larson–Miller parameter plot of time-to-rupture thermal creep data for 12YWT, MA957 and advanced 9Cr-WMoVNb tempered martensitic steel. The results show that the creep properties of 12YWT and MA957 are improved by 2–5 orders of magnitude over the 9Cr-WMoVNb as determined from the combination of time-to-failure and temperature at any given stress. Furthermore, the microstructural analysis of creep specimens after failure has shown that the nanoclusters are very stable for long periods of time at elevated test temperatures and stresses [83–85]. In these

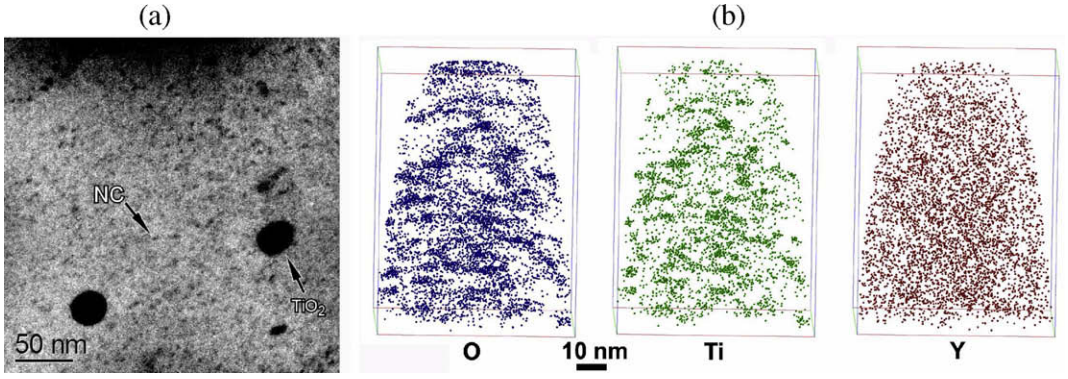

Fig. 8. The Ti-, Y-, and O-enriched nanoclusters (NC) present in the 14YWT ferritic alloy: (a) EFTEM Fe–M jump ratio map and (b) LEAP element maps of Cr, Y, Ti and O atoms [72].

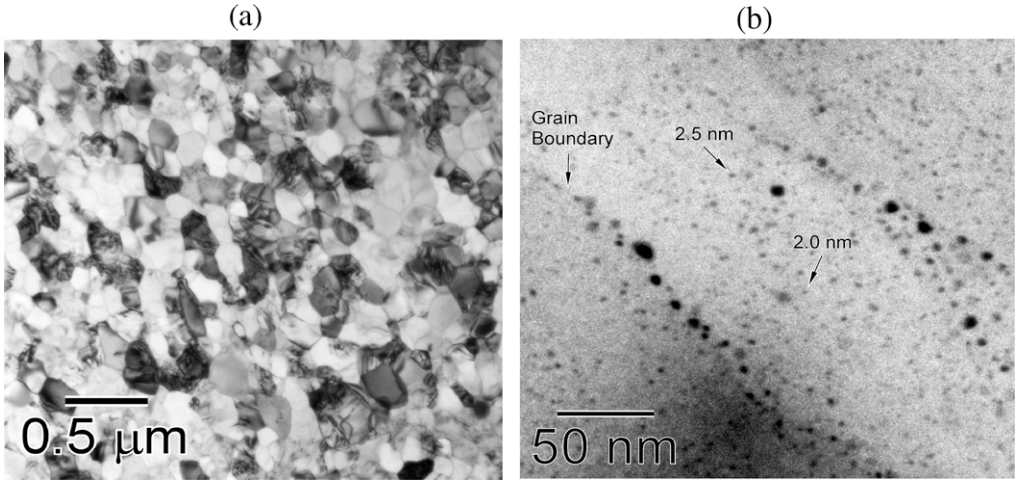

Fig. 9. The nano-size grain structure in the 14 YWT ferritic alloy: (a) bright field TEM image and (b) EFTEM Fe–M jump ratio map.

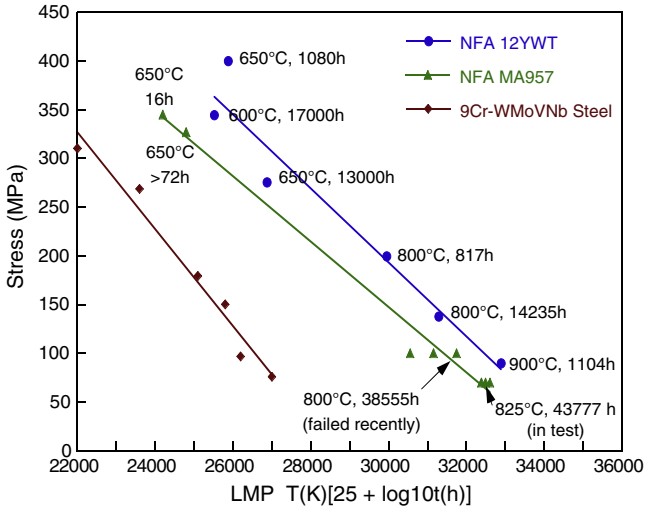

Fig. 10. Larson–Miller parameter time-to-rupture creep data for 12YWT, MA957, and 9Cr-WMoVNb alloys [78,81,82].

studies, the nanoclusters showed essentially no change in size after 14,500 h exposures at 800 °C and 138 MPa for 12YWT and, even more remarkably, after 38,555 h at 800 °C and 100 MPa for a recently failed specimen of MA957. These results indicate that the dispersion of nanoclusters is an attractive approach to strengthen structural alloys at elevated temperatures and to stabilize the microstructure during long term exposure in thermal creep environments.

It is envisioned that the high number density of nanoclusters and fine grain size present in the 14YWT alloy will form a high sink strength for the trapping of point defects and He atoms generated during neutron irradiation. The high interfacial area of the nanoclusters and high grain boundary surface area of the small grains can capture segregating self-interstitial atoms and vacancies and catalyze their recombination [86]. Achieving a high number density of nanoclusters, i.e. $\sim 1 \times 10^{24}\,m^{-3}$ means that the effective spacing between nanoclusters is on the order of 10–15 nm, which increases the probability of capturing the segregating point defects. The nanoclusters may also trap transmutation-produced He and prevent it from migrating to grain boundaries and nucleating cavities. Helium trapping at particle-matrix interfaces has been demonstrated in several phosphorous-modified austenitic stainless steels; the development of a fine dispersion of phosphide particles has been shown to be an effective means of delaying the transition to steady-state swelling [87,88]. Recent results obtained from the microstructural analysis of MA957 following neutron irradiation to 9 dpa at 500 °C with ~380 appm He implanted uniformly to a depth of ~5–8 μm in TEM specimens, provide strong evidence that point defects and He atoms migrate to and are trapped by the nanoclusters [86]. In this study, the EFTEM analysis revealed that the nanoclusters were unaffected by the radiation damage and comparison with through-focus images found it difficult to reliably detect nano-size He bubbles in the microstructure. Interestingly, while the number density of nanoclusters in 14YWT and MA957 are similar, the grain size in 14YWT is much smaller than that in the MA957 sample that was used in the neutron irradiation experiment. Measurements show that the grain size for 14YWT can be as small as 136 ± 14 nm with a grain aspect ratio of ~1.2 and for MA957 the grain size is 654 ± 79 nm with a grain aspect ratio of ~3. This suggests that the point defect sink strength of 14YWT may be even higher than that of MA957 based on the total surface area of the combined interfacial area of nanoclusters and grain boundary surface area.

Based on these encouraging results, it is suggested that a similar approach could be adapted to fcc Ni-base alloy systems in order to improve the radiation-tolerance and increase high-temperature strength. A project combining theoretical modeling with experimental studies to understand the formation and stability of nanoclusters in Ni was recently initiated [89]. The theoretical modeling consists of first-principles approach for calculating the binding energies between solute atoms and vacancies, which have been identified as having a vital role in the formation of nanoclusters in bcc Fe [90]. The experimental study will investigate two particle dispersions in unalloyed Ni, one based on Ti, Y, and O atoms and the other on Zr, La, and O atoms. The typical approach for dispersing oxide particles in Ni alloys involves mechanical alloying oxide powders, such as Y_2O_3, with atomized powders of Ni-based superalloys [91–93]. This approach can complicate the processing conditions for forming nano-size oxide particle dispersions due to the high alloying content of Ni-based superalloys. The approach of the present study is to ball mill appropriate powders containing Ti, Y, and O or Zr, La, and O atoms with high purity Ni powder. The milled powders were then annealed at 800 °C or hot pressed

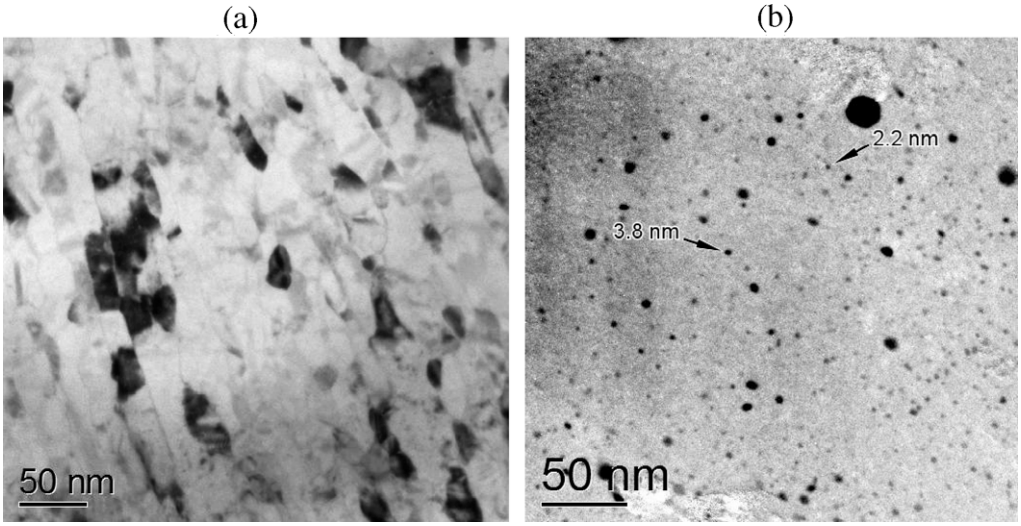

Fig. 11. Nano-scale grain and particle dispersions in the fcc dilute Ni alloy containing Zr, La and O: (a) bright field image of ball-milled powder and (b) EFTEM Ni–M jump ratio image of the nano-size particle dispersion developed in the 950 °C hot-pressed powder.

at 950 °C. Preliminary results showing the characteristics of the grain size and particle dispersion obtained in the Zr, La, and O containing Ni alloy is shown in Fig. 11. Fig. 11(a) shows that a very small grain size is formed in the dilute Ni alloy powder after ball milling. The grains are less than 50 nm in size and are slightly elongated due to the severe deformation caused by the large transfer of energy from the high frequency of ball-powder impacts during ball milling. Upon annealing or hot pressing, a high number density of nano-size particles precipitated in the Ni lattice. Fig. 11(b) shows the EFTEM Ni–M jump ratio image that was obtained from the hot pressed powders. The nano-size particles show dark contrast indicating that the particles are depleted in Ni. Corresponding EFTEM composition maps confirmed that the nano-size particles contained O, Zr, and La. However, this method is not suitable for quantitative analysis of the particle composition. Measurements of the particle size and number density indicate that the size ranged from ~2 to ~8 nm diameter (fewer larger oxide particles were also observed) and the number density was $\sim 3 \times 10^{23}\ m^{-3}$. The microstructural characterization also showed that the oxygen-rich particles were not as uniformly distributed in the dilute Ni alloy as in the 14YWT ferritic alloy. Nevertheless, the preliminary results of this study are promising since they show that a high number density of nano-size particles can be produced in fcc Ni by the mechanical alloying method. Further work is in progress to investigate the composition, structure and thermal stability of the nano-size particles.

9. Summary

Neutron irradiation data have been summarized for a group of Ni-base alloys investigated as potential cladding and duct materials for the LMFBR programs in the US and EU. Selected data have been used to illustrate the complex range of mechanisms involved in the radiation-induced reduction in high temperature ductility and also to illustrate the early transition that occurs from incubation to steady state swelling in some alloys.

Depending upon alloy composition and the initial heat treatment, the loss of high temperature ductility has been associated with a variety of grain boundary phenomena including radiation-enhanced precipitation of intermetallic and carbide phases with plate morphologies, segregation of solutes and precipitation of continuous films of gamma prime, segregation of impurity elements such as S and P, and the precipitation and stress-induced growth of helium bubbles. Low ductility trans-granular failures have also been observed associated with the radiation-enhanced formation of intermetallic phases with plate morphologies and the initiation of fracture at the particle-matrix interface induced by channel deformation in the hardening regime.

When thermal precipitation behavior is dominated by the formation of coarse distributions of complex carbide phases such as $M_{23}C_6$ and M_6C, there is a very strong probability that the radiation-enhanced precipitation of these phases will accelerate the transition from the swelling incubation regime into steady-state swelling, regardless of Ni content.

These radiation-induced phenomena will certainly manifest themselves to some degree in each of the Ni-base alloys currently being considered for Gen IV applications in fast neutron, mixed spectrum and thermal neutron environments. The characteristics of ductility loss will depend upon alloy composition and microstructure, neutron dose, damage rate and neutron spectrum and on the conditions of temperature and applied stress. The importance of component design in minimizing potential embrittlement cannot be over-emphasized since it may be possible to avoid the combination of stress and temperature conditions required to activate a given failure mechanism. A case in point is the high burn-up levels achieved with PE-16 clad fuel pins in the EU fast breeder reactor program where careful fuel pin design took advantage of the moderate levels of void swelling to maintain cladding stresses below the level needed to induce grain boundary helium bubble growth.

There are currently no irradiation data on candidate materials such as Alloy 230, and Alloy 120, although some initial low dose data for Alloy 617 were presented recently [94]. The limited data on Alloy 800 and on Hastelloy X indicate that both are susceptible to radiation-induced ductility loss under certain conditions and that both alloys are prone to loss of swelling resistance related to the precipitation of complex carbide phases and the co-operative growth of associated voids.

Because of the susceptibility of commercial Ni-base alloys to damaging phenomena related to radiation-induced segregation, radiation-enhanced phase instabilities and radiation-induced helium bubble and void formation, it is imperative to pursue a comprehensive assessment of the potential irradiation behavior of the Gen IV candidate alloys in parallel with the conventional structural stability and mechanical behavior programs. The existing data from the earlier LMFBR alloy development programs and basic radiation effects programs provide an excellent basis for such an assessment which needs to be combined with the development of kinetic and thermodynamic models of phase stability incorporating the effects of high vacancy concentrations, the radiation-induced segregation of various species to grain boundary and matrix sinks and the behavior of transmutation-generated helium. The principal objective would be to identify potentially damaging radiation-induced phenomena, confirm their existence with low-dose neutron irradiation experiments and to develop mitigation strategies based upon compositional and microstructural modifications of existing alloys.

A longer-range alternative to the modification of existing commercial alloys is the design of completely new alloys utilizing the principal of creating a high number density of stable nano-scale clusters or particles, thereby establishing a very high density of point defect recombination sites and traps for helium atoms. Considerable progress in this direction has been demonstrated for the ferritic and ferritic–martensitic alloy systems based upon mechanical alloying. Efforts are in progress to adapt a similar approach to the design and development of high strength, radiation-stable Ni-base alloys.

Acknowledgement

Research sponsored by the US Department of Energy, under contract DE-AC05-00OR22725 with UT-Battelle, LLC.

References

[1] G.O. Hayner et al., Next Generation Nuclear Plant Materials Selection and Qualification Program Plan, Idaho National Engineering Laboratory Report INEEL/EXT-03-001128, (Rev0), Idaho Falls, Idaho, November, 2003.
[2] J. Buongiorno et al., Supercritical Water Reactor (SCWR) Survey of Materials Experience and R&D Needs to Assess Viability, Idaho National Engineering Laboratory Report, INEEL-EXT-03-00693 (Rev1), Idaho Falls, Idaho, September, 2003.
[3] W.R. Corwin et al., The Gas Cooled Fast Reactor (GFR) Survey of Materials Experience and R&D Needs to Assess Viability, Oak Ridge National Laboratory Report ORNL/TM2004/99, Oak Ridge Tennessee, 2004.
[4] R.E. Stoller, L.K. Mansur, Modeling and Microstructural Analysis: Needs and Requirements for Generation IV Fission Reactors, Oak Ridge National Laboratory Report ORNL/TM-2003/242, Oak Ridge, Tennessee, May, 2004.
[5] L.K. Mansur et al., J. Nucl. Mater. 329–333 (2004) 166.
[6] T. Allen et al. (Eds.), High Temperature Materials Workshop, ANL-02/12, Argonne National Laboratory, August, 2002.
[7] B.A. Chin et al., Nucl. Technol. 57 (1982) 426.
[8] J.L. Straalsund, R.W. Powell, B.A. Chin, J. Nucl. Mater. 108&109 (1982) 299.
[9] A.L. Ward et al., in: F.R. Schober, J.A. Sprague (Eds.), Irradiation Effects on Microstructure and Properties of Metals, ASTM STP 611, American Society for Testing and Materials, Philadelphia, 1976, p. 156.

[10] T.T. Claudson, H.J. Pessel, in: Flow and Fracture of Metals and Alloys in Nuclear Environments, ASTM STP 380, American Society of Testing and Materials, Philadelphia, 1965.
[11] J. Moteff et al., J. Nucl. Mater. 17 (1965) 245.
[12] T.T. Claudson, in: W.L.R. Rice (Ed.), Effects of Irradiation on Structural Materials, ASTM STP 426, American Society for Testing Materials, Philadelphia, 1976, p. 67.
[13] F.A. Comprelli et al., in: A.L. Bement (Ed.), Irradiation Effects on Structural Alloys for Thermal and Fast Reactors, ASTM STP 457, American Society for Testing and Materials, Philadelphia, 1969, p. 400.
[14] H. Bohm, K.D. Kloss, in: M.L. Bleiberg, J.W. Bennett (Eds.), Radiation Effects in Breeder Reactor Structural Materials, TMS-AIME, New York, 1977, p. 347.
[15] J.T. Busby, Advanced Structural Materials Development for Advanced Fast Reactor Systems: Strategic Plan, Oak Ridge National Laboratory Report, ORNL/TM/GNEP/07-01, September, 2007.
[16] K. Ehrlich et al., J. Nucl. Mater. 327 (2004) 140.
[17] T.M. Angeliu et al., J. Nucl. Mater. 366 (2007) 223.
[18] W.J.S. Yang et al., J. Nucl. Mater. 108&109 (1982) 339.
[19] E.H. Lee, L.K. Mansur, J. Nucl. Mater. 278 (2000) 1.
[20] E.H. Lee, L.K. Mansur, J. Nucl. Mater. 278 (2000) 11.
[21] E.H. Lee, L.K. Mansur, J. Nucl. Mater. 278 (2000) 20.
[22] E.H. Lee, L.K. Mansur, Phil. Mag. A52 (1985) 493.
[23] X.S. Xie, J.X. Dong, M.C. Zhang, S.H. Fu, Mater. Sci. Forum 546–549 (Part 3) (2007) 1281.
[24] C. Slama, M. Abdellaoui, J. Alloy. Compd. 306 (2000) 277.
[25] M. Sundaraman et al., in: E.A. Loria (Ed.), Superalloys 718, 625, 706 and Various Derivatives, The Minerals, Metals, and Materials Society, 1997, p. 367.
[26] M.K. Miller et al., Mater. Sci. Eng. A270 (1999) 14.
[27] J.A. Horak et al., US Department of Energy National Cladding/Duct Materials Development Quarterly Progress Report, TC-160-27, 1980, p. 235.
[28] A.F. Rowcliffe, J.A. Horak, Trans. ANS 38 (1981) 226.
[29] G.R. Gessel et al., DOE Cladding/Duct Materials Development Quarterly Progress Report, TC-160-18, 1978, p. 196.
[30] S. Vaidyanathan et al., in: H.R. Brager, J.S. Perrin (Eds.), Effects of Irradiation on Structural Materials, ASTM STP 782, American Society for Testing and Materials, Philadelphia, 1982, p. 619.
[31] F.H. Huang, R.L. Fish, in: F.A. Garner, J.S. Perrin (Eds.), Effects of Radiation on Materials, ASTM STP 870, American Society for Testing of Materials, Philadelphia, 1985, p. 720.
[32] B.J. Makenas et al., Trans. Am. Nucl. Soc. 44 (1983) 258.
[33] W.J.S. Yang, B.J. Makenas, in: F.A. Garner, J.S. Perrin (Eds.), Effects of Radiation on Materials, ASTM STP 870, vol. II, American Society for Testing and Materials, Philadelphia, 1985, p. 127
[34] G.H. Broomfield, in: Irradiation Effects in Structural Alloys for Thermal and Fast Reactors, ASTM STP 457, American Society for Testing and Materials, Philadelphia, 1965, p. 38.
[35] A.F. Rowcliffe et al., in: Effects of Radiation on Structural Metals, ASTM STP 426, American Society for Testing and Materials, Philadelphia, 1967, p. 161.
[36] R.D. Nicholson, R.B. Jones, in: Effects of Radiation on Materials, ASTM STP 683, American Society for Testing and Materials, Philadelphia, 1979, p. 529.
[37] R. Bajaj et al., in: D. Kramer, H.R. Brager, J.S. Perrin (Eds.), Effects of Radiation on Materials, ASTM STP 725, American Society for Testing and Materials, Philadelphia, 1981, p. 326.
[38] W.J.S. Yang, J. Nucl. Mater. 132 (1985) 249.
[39] A.L. Chang, Micro and Macro Mechanics of Crack Growth, Met. Soc. AIME, Warrendale, Pa, 1982.
[40] R.M. Boothby, D.R. Harries, Mechanical Behavior and Nuclear Applications of Stainless Steel at Elevated Temperatures, Metals Society, London, 1982.
[41] R.M. Boothby, J. Nucl. Mater. 230 (1996) 148.
[42] E.D. Hyam, G. Sumner, Radiation Damage in Solids, vol. 1, IEA, Vienna, 1962.
[43] C. Brown, V. Levy, J.L. Seran, K. Ehrlich, R. Roger, H. Bergmann, in: Proceedings of the International Conference on Fast Reactor and Related Fuel Cycles, Kyoto, vol. 1, 1991, p. 751.
[44] M. Naganuma et al., in: Proceedings of the IEA Conference on MOX Fuel Cycle Technologies for Medium and Long Term Deployment, IAEA, 2000, p. 556.
[45] K.F. Allbeson et al., Nucl. Eng. 37 (3) (1990) 87.
[46] P. Martin et al., Nucl. Technol. 161 (2008) 35.
[47] W.G. Johnston et al., J. Nucl. Mater. 54 (1974) 24.
[48] J.F. Bates, W.G. Johnston, in: Proceedings of the International Conference on Radiation Effects in Breeder Reactor Structural Materials, Scottsdale, The Metallurgical Society of AIME, New York, 1977, p. 625.
[49] A.D. Brailsford, L.K. Mansur, J. Nucl. Mater. 71 (1977) 110.
[50] F.A. Garner, in: B.R.T. Frost (Ed.), Materials Science and Technology, Nuclear Materials, vol. 10A, Part 1, 1994, p. 420.
[51] F.A. Garner, H.R. Brager, in: F.A. Garner, J.S. Perrin (Eds.), Effects of Radiation on Materials, ASTM STP 870, American Society for Testing and Materials, Philadelphia, 1985, p. 187.
[52] L.K. Mansur, Phil. Mag. A44 (1981) 867.
[53] F.A. Garner, D.S. Gelles, in: N.H. Packan, R.E. Stoller, A.S. Kumar (Eds.), Effects of Radiation on Materials, ASTM STP 1046, American Society for Testing and Materials, Philadelphia, vol. 2, 1990, p. 673.
[54] W.K. Appleby et al., J. Nucl. Mater. 43 (1972) 213.
[55] J.C. Zhao et al., Mater. Sci. Eng. A293 (2000) 112.
[56] K. Bhanu et al., Scripta Met. Mater. 31 (1994) 381.
[57] E.H. Lee et al., in: J.R. Holland, L.K. Mansur, D.I. Potter (Eds.), Phase Stability during Irradiation, Metallurgical Society of AIME, 1980, p. 191.
[58] W.J. Ren, R.W. Swindeman, High Temperature Metallic Materials Test Plan for Generation IV Nuclear Reactors, ORNL/TM-2004, Oak Ridge National Laboratory, November, 2004
[59] H. Kirchover et al., Nucl. Technol. 66 (1984) 139.
[60] J.-C. Zhao et al., Mater. Sci. Eng. A293 (2000) 112.
[61] N. Saunders, A.P. Miodownik, CALPHAD: Calculation of Phase Diagrams, A Comprehensive Guide, Elsevier Science Ltd., Oxford, United Kingdom, 1998.
[62] N. Saunders et al., in: Superalloys 2004, Minerals Metals and Materials Society, 2004, p. 8490.
[63] G. Palumbo et al., Mater. Res. Symp. Proc. Materials Research Society 458 (1997) 273.
[64] L. Tan et al., J. Nucl. Mater. 371 (2007) 171.
[65] L. Tan et al., J. Nucl. Mater. 374 (2008) 270.
[66] B.A. Thiele et al., J. Nucl. Mater. 171 (1990) 94.
[67] R.K. Nanstad et al., J. Nucl. Mater., these proceedings.
[68] M. Vittori, J. Mater. Sci. 16 (1981) 3461.
[69] S. Ukai et al., J. Nucl. Mater. 307–311 (2002) 749.
[70] D.S. Gelles, J. Nucl. Mater. 237 (1996) 293.
[71] S. Yamashita, J. Nucl. Mater. 367–370 (2007) 202.
[72] M.K. Miller, K.F. Russell, D.T. Hoelzer, J. Nucl. Mater. 351 (2006) 261.
[73] D.T. Hoelzer et al., J. Nucl. Mater. 367–370 (2007) 166.
[74] D.A. McClintock, Mechanical Properties of an Irradiated Nanocluster Strengthened High-chromium Ferritic Alloy, PhD Dissertation, Univ. Texas at Austin, TX, 2008.
[75] M.J. Alinger, G.R. Odette, D.T. Hoelzer, J. Nucl. Mater. 329–333 (2004) 382.
[76] M.K. Miller et al., Shanghai Met. 30 (2008) 1 (in Chinese).
[77] J. Bentley et al., Microsc. Microanal. 10 (2) (2004) 662.
[78] M.K. Miller, Atom Probe Tomography, Kluwer Academic/Plenum, New York, 2000.
[79] D.A. McClintock et al., J. Nucl. Mater. 386–388 (2009) 307.
[80] I.-S. Kim et al., ISIJ Int. 43 (2003) 1640.
[81] J.J. Fisher, US Patent 4,075,010, issued February, 1978.
[82] R.L. Klueh et al., J. Nucl. Mater. 341 (2005) 103.
[83] M.K. Miller et al., J. Nucl. Mater. 329–333 (2004) 338.
[84] M.K. Miller et al., Mater. Sci. Eng. A353 (2003) 140.
[85] D.T. Hoelzer et al., The Microstructural Stability of a Ruptured Thermal Creep Specimen of MA957, 2008DOE/ER-0313/44, June 30, 2008, p. 53.
[86] T. Yamamoto et al., J. Nucl. Mater. 367–370 (2007) 399.
[87] L.K. Mansur, J. Nucl. Mater. 83 (1979) 109.
[88] E.H. Lee, L.K. Mansur, Phil. Mag. A61 (1990) 733.
[89] D.T. Hoelzer et al., Design of Point Defect Trapping Centers in Nanostructured Nickel for Advanced Nuclear Applications, ORNL Laboratory Directed Research and Development (LDRD), D07-139, 2007–2008.
[90] C.L. Fu, Maja Krčmar, G.S. Painter, Xing-Qiu Chen, Phys. Rev. Lett. 99 (225502) (2007) 1.
[91] M. Rühle, T. Steffens, Z. Metallkd. 83 (1992) 436.
[92] H.K.D.H. Bhadeshia, Mater. Sci. Technol. 16 (2000) 1404.
[93] T.C. Totemeier, T.M. Lillo, Metall. Mater. Trans. A36 (2005) 785.
[94] R.K. Nanstad et al., J. Nucl. Mater. 392 (2009) 331.